The DOI for this manuscript is doi: 10.1175/JCLI-D-11-00627.1

The final published version of this manuscript will replace the preliminary version at the above DOI once it is available.

If you would like to cite this EOR in a separate work, please use the following full citation:

Li, Z., W. Yu, T. Li, M. VSN, and F. Tangang, 2012: Bimodal character of cyclone climatology in Bay of Bengal modulated by monsoon seasonal cycle. J. Climate. doi:10.1175/JCLI-D-11-00627.1, in press.

Bimodal character of cyclone climatology in Bay of Bengal modulated by monsoon seasonal cycle

Zhi Li[1], Weidong Yu[1], Tim Li[2], VSN Murty[3] and Fredolin Tangang[4]

1. Center for Ocean and Climate Research, First Institute of Oceanography, SOA, Qingdao 266061, China

2. IPRC and Department of Meteorology, University of Hawaii, Honolulu, Hawaii, USA

3. National Institute of Oceanography, Regional Centre, Visakhapatnam 530 017, India

4. Research Centre for Tropical Climate Change System, Universiti Kebangsaan Malaysia, 43600 Bangi Selangor, Malaysia

Submitted to J. Climate on Oct. 25, 2011

Revised on August 8, 2012

Corresponding author: Weidong Yu, First Institute of Oceanography, SOA, Qingdao 266061, China. E-mail: wdyu@fio.org.cn

Abstract

The annual cycle of tropical cyclone (TC) frequency over the Bay of Bengal (BoB) exhibits a notable bimodal character, different from a single peak in other basins. The causes of this peculiar feature were investigated through the diagnosis of a genesis potential index (GPI) with the use of the NCEP reanalysis I dataset during the period 1981-2009. A methodology was developed to quantitatively assess the relative contributions of four environmental parameters. Different from a conventional view that the seasonal change of vertical shear causes the bimodal feature, we found that the strengthened vertical shear alone from boreal spring to summer cannot overcome the relative humidity effect. It is the combined effect of vertical shear, vorticity and SST that leads to the GPI minimum in boreal summer. It is noted that TC frequency in October-November is higher than that in April-May, which is primarily attributed to the difference of mean relative humidity between the two periods. In contrast, more super cyclones (Category 4 or above) occur in April-May than in October-November. It is argued that greater ocean heat content, the first branch of northward propagating intra-seasonal oscillations (ISOs) associated with the monsoon onset over the BoB, and stronger ISO intensity in April-May are favorable environmental conditions for cyclone intensification.

1. Introduction

Tropical cyclones (TCs) are severe weather systems that involve air-sea interactions over warm oceans during the summer season. They span the global tropics with several activity centers (Fig. 1) over the Arabian Sea (AS), Bay of Bengal (BoB), Western North Pacific (WNP), Eastern North Pacific (ENP), Northern Atlantic (NATL), Southern Indian Ocean (SIO) and Western South Pacific (WSP). TCs draw intense scientific and social interest concerns due to the following three reasons. Firstly, they contribute importantly to the overall summer season rainfall in regions such as WNP. Secondly they play a key role in modulating the inter-annual variations of the regional rainfall (Lyon et al. 2006; Lyon and Camargo 2008) while TCs are also modulated by large-scale variability (Li 2012). Thirdly, their frequency, intensity and track may change due to global warming (Webster et al. 2005; Emanuel 2005; Landsea et al. 2006; Li et al. 2010).

The BoB hosts the majority of North Indian Ocean (NIO) TCs. Statistical analysis reveals that there are a total of 150 TCs during the period of 1981-2009 in the NIO, among which about 2/3 of typhoons and 4/5 of super typhoons (Category 4 or above) formed in the BoB. Considering the dense population around the BoB, strong TCs can sometimes cause catastrophic destruction when they make land. In fact, the BoB is the region where the deadliest TCs occurred and the BoB-rim countries such as India, Bangladesh and Myanmar mostly suffer from these devastating cyclones. In the historical cyclone records, seven of the top ten deadliest cyclones formed in the BoB and the most recent example is cyclone Nargis (Webster 2008; Kikuchi et al.

2009; Lin et al. 2009; McPhaden et al. 2009; Yanase et al. 2010), which hit the southern coast of Myanmar on May 2, 2008 and caused the worst natural disaster in the recorded history of Myanmar.

From the climatological point of view, TCs in the BoB have distinct features and exhibit strong differences from those in other basins (Camargo et al. 2007; Kikuchi and Wang 2010; Yanase et al. 2011; Evan and Camargo 2011). The annual cycle of BoB TCs is characterized by the prominent double peaks occurred during the monsoon transition periods (April-May and October-November) while the single peak is dominant during the corresponding solar summer in the WNP, WSP, ENP, NATL and SIO (Fig. 2). The TC climatology in the AS shows the similar feature to that in the BoB, but with much less TCs. Evan and Camargo (2011) recently gave a detailed documentation of AS cyclone climatology. Hence the present analysis mainly focuses on the BoB, while some analysis on other basins is also included for purpose of comparison. It is furthermore noteworthy that in addition to the annual cycle, the TC genesis activity in the BoB is also strongly modulated by the tropical intraseasonal oscillation (ISO) (Kikuchi and Wang 2010; Yanase et al. 2010, 2012). While more cyclones occur during the second peak period (October-November), the major fraction of strong cyclones (over category 4) usually occur in the first peak season (April) just before the southwest monsoon onset.

The aim of present paper is two-fold. Firstly, we will illustrate large-scale environmental controlling processes with relevance to the bimodal feature of BoB TC climatology, with a particular emphasis on their quantitative contributions in different seasons. Secondly, we will explain the predominance of strong cyclones (category 4 or above) in April and its relation with the southwest monsoon onset.

The rest of the paper is organized as follows. In section 2, we introduce the data and its analysis method. The influence of the large scale environmental factors on BoB cyclone genesis is diagnosed in section 3 and the comparison with other basins is described in section 4. The observed upper limit of the background vertical shear for TC formation is discussed in section 5. Section 6 is devoted to understanding the predominance of strong TCs during the first peak. Finally we summarize the major results and include a discussion.

2. Data and method

TC best track data from the Joint Typhoon Warning Center (JTWC) were used to determine the TC genesis and development in the BoB, WNP, ENP, NATL, SIO and WSP. Monthly wind, air temperature, air specific humidity and relative humidity and daily wind data from NCEP/NCAR reanalysis, monthly SST from NOAA OI data sets and NOAA daily outgoing long-wave radiation (OLR) are used here to describe the large scale environmental processes. Except for the SST data that have a horizontal resolution of 2^{o} latitude by 2^{o} longitude, the other data have a resolution of 2.5^{o} latitude by 2.5^{o} longitude.

It is well known that cyclone genesis depends on several environmental factors (Gray 1968, 1979), including (i) low-level relative vorticity, (ii) Coriolis parameter (at least a few degrees poleward of the equator), (iii) vertical shear of the horizontal winds, (iv) sea surface temperature (SST) threshold (usually taken 26°C), (v) conditional instability through a deep atmospheric layer, and (vi) humidity in the lower and middle troposphere. While much is known about the influencing factors of cyclone genesis, a quantitative theory is lacking. In the absence of such a theory, empirical methods are necessary and useful. Gray (1979) developed an index to quantitatively describe the influences of the large scale environmental factors on cyclone genesis. Emanuel and Nolan (2004) further refined the TC genesis potential index (GPI) and Carmago et al. (2007) used this index to diagnosis the ENSO modulation of cyclone genesis.

Following Emanuel and Nolan (2004), we use the GPI as our main diagnosis tool, which is represented by

$$\mathrm{GPI} = \mathrm{Term1} \times \mathrm{Term2} \times \mathrm{Term3} \times \mathrm{Term4} \qquad (1)$$

Where Term1=$|10^5\eta|^{3/2}$, Term2=$(1+0.1V_{shear})^{-2}$,Term3=$(H/50)^3$, Term4=$(V_{pot}/70)^3$, η is the absolute vorticity at 850 hPa, V_{shear} is the magnitude of the vertical wind shear between 850 hPa and 200 hPa, H is the relative humidity at 600 hPa, V_{pot} is the maximum TC potential intensity defined by Emanuel (1986, 1987, 1988, 1995, 2000):

$$V_{pot}^2 = C_p(T_s - T_o)\frac{T_s}{T_o}\frac{C_k}{C_D}(\ln\theta_e^* - \ln\theta_e)$$

In the potential intensity (PI) formula above, C_p is the heat capacity at constant pressure, T_s is the ocean temperature, T_o the mean outflow temperature, C_k the exchange coefficient for enthalpy, C_D the drag coefficient, θ_e^* the saturation equivalent potential temperature at ocean surface, and θ_e the boundary layer equivalent potential temperature.

3. Cause of the bimodal annual cycle in the BoB

The monthly occurrence number of TCs based on JTWC best track data in seven major TC active regions is shown in Fig. 2. Consistent with previous studies (Gray 1968; Camargo et al. 2007; Evan and Camargo 2011), there is a marked difference in the TC genesis frequency between the BoB (and AS) and other ocean basins. TC frequency in the BoB has two peaks in monsoon transition periods (April-May and October-November), while very low genesis frequency occurs during the strong southwest monsoon period (June-July-August-September). Previous studies (e.g., Gray 1968; Camargo et al. 2007; Evan and Camargo 2011; Yanase et al. 2012) suggested that the bimodal feature of TC frequency in the BoB and AS is attributed to the annual cycle of the background vertical shear as strong vertical shear in boreal summer prevents TC formation. Here we will develop a quantitative diagnosis method to reveal the relative roles of large-scale environmental factors in causing the bimodal feature.

Using the NCEP monthly reanalysis data for 1981-2009, we calculate the box-averaged climatological monthly GPIs for the seven regions as shown in Fig. 1. The size of each box is defined as follows: (10-20^{o}N, 67-75^{o}E) for the AS, (5-15^{o}N, 80-95^{o}E) for the BoB, (5-20^{o}N, 130-150^{o}E) for the WNP, (10-20^{o}N, 240-260^{o}E) for the ENP, (10-20^{o}N, 310-340^{o}E) for the NATL, (10-25^{o}S, 55-100^{o}E) for the SIO and (10-25^{o}S, 160^{o}E -170^{o}W) for the SWP. As shown in Fig. 2, the GPI index well captures the annual cycle pattern in all regions, especially the double peaks in the

BoB.

Figure 2 shows that GPI represents well the combined effect of the four large-scale environmental processes on the cyclone genesis. Next we further investigate the relative contributions of each individual factor. Camargo et al. (2007) first made such an attempt in their study on the interannual variations of the cyclone genesis and this method was then used in the intra-seasonal variations of the cyclone genesis (Camargo et al. 2009). Here we will use the similar method with some modifications to study the seasonal cycle of cyclone genesis, specifically identifying the individual contribution from the four large-scale environmental processes. This analysis will enable us to better understand the formation of the bimodal feature of BoB TC climatology. The modified method is explained as below.

Taking a natural logarithm operating on both sides of equation (1), one may obtain:

$$\begin{aligned}\ln \mathrm{GPI} &= \ln(\mathrm{Term1} \times \mathrm{Term2} \times \mathrm{Term3} \times \mathrm{Term4}) \\ &= \ln(\mathrm{Term1}) + \ln(\mathrm{Term2}) + \ln(\mathrm{Term3}) + \ln(\mathrm{Term4}) \qquad (2)\end{aligned}$$

Applying total differential at both sides of equation (2) yields

$$\frac{\mathrm{dGPI}}{\mathrm{GPI}} = \frac{\mathrm{dTerm1}}{\mathrm{Term1}} + \frac{\mathrm{dTerm2}}{\mathrm{Term2}} + \frac{\mathrm{dTerm3}}{\mathrm{Term3}} + \frac{\mathrm{dTerm4}}{\mathrm{Term4}} \qquad (3)$$

Substituting (1) into (3), we have

$$\begin{aligned}\mathrm{dGPI} = &\ \mathrm{dTerm1} \times \mathrm{Term2} \times \mathrm{Term3} \times \mathrm{Term4} \qquad (4) \\ &+ \mathrm{dTerm2} \times \mathrm{Term1} \times \mathrm{Term3} \times \mathrm{Term4} \\ &+ \mathrm{dTerm3} \times \mathrm{Term1} \times \mathrm{Term2} \times \mathrm{Term4} \\ &+ \mathrm{dTerm4} \times \mathrm{Term1} \times \mathrm{Term2} \times \mathrm{Term3}\end{aligned}$$

Integrating equation (4) from annual mean to a particular month, one may obtain the following equation:

$$\delta\mathrm{GPI} = \mathrm{t1} + \mathrm{t2} + \mathrm{t3} + \mathrm{t4} \qquad (5)$$

$$= \alpha_1 \cdot \delta\mathrm{Term1} + \alpha_2 \cdot \delta\mathrm{Term2} + \alpha_3 \cdot \delta\mathrm{Term3} + \alpha_4 \cdot \delta\mathrm{Term4}$$

where

$$\begin{cases} \alpha_1 = \overline{\mathrm{Term2}} \cdot \overline{\mathrm{Term3}} \cdot \overline{\mathrm{Term4}} \\ \alpha_2 = \overline{\mathrm{Term1}} \cdot \overline{\mathrm{Term3}} \cdot \overline{\mathrm{Term4}} \\ \alpha_3 = \overline{\mathrm{Term1}} \cdot \overline{\mathrm{Term2}} \cdot \overline{\mathrm{Term4}} \\ \alpha_4 = \overline{\mathrm{Term1}} \cdot \overline{\mathrm{Term2}} \cdot \overline{\mathrm{Term3}} \end{cases}$$

or

$$\begin{cases} \alpha_1 = \overline{\mathrm{Term2} \cdot \mathrm{Term3} \cdot \mathrm{Term4}} \\ \alpha_2 = \overline{\mathrm{Term1} \cdot \mathrm{Term3} \cdot \mathrm{Term4}} \\ \alpha_3 = \overline{\mathrm{Term1} \cdot \mathrm{Term2} \cdot \mathrm{Term4}} \\ \alpha_4 = \overline{\mathrm{Term1} \cdot \mathrm{Term2} \cdot \mathrm{Term3}} \end{cases}$$

and

$$\delta\mathrm{GPI} = \mathrm{GPI} - \overline{\mathrm{GPI}} \quad .$$

In equation (5), a bar denotes an annual mean value, and δ represents the difference between an individual month and the annual mean. An approximation has been made in deriving equation (5) by assuming constant coefficients for α_1, α_2, α_3 and α_4.

Figure 3 shows the diagnosed results from both the left-hand side and the right-hand side of equation (5). Different color bars in Fig. 3 represent the contributions from the four environmental factors in each month. Calculations with two different approximations listed above for the components used to determine coefficients α_1, α_2, α_3 and α_4 show that the results are quite close (see the solid line and the gray dash line in Fig. 3). The sum of the four right-hand-side diagnosed terms matches well the observed value of the left-hand side term, which gives us confidence to further use this decomposition to understand the relative contribution of the individual terms. It is clearly illustrated that the minimum of the GPI in boreal summer over the BoB is primarily attributed to the environmental vertical shear and the absolute vorticity, although the relative humidity tends to enhance the TC frequency in summer.

To clarify the dominant processes that shape the mean seasonal cycle of the cyclone frequency, especially its abrupt increase or decrease, we apply the diagnosis procedure expressed by the equation (5) based on two-month sequence data. The contribution from four individual processes and their percentage are listed in Table 1.

The first increase of cyclone frequency occurs in April-May compared with the level in February-March (Figs. 2 and 3). The key process responsible for such a rapid increase is the abrupt increase of the mid-level atmosphere relative humidity. It plays the dominant role and contributes 87% of the total GPI increase (Table1). No competing factors occur during this period. It is well understood that April-May is the pre-monsoon period, when the oceanic and atmospheric conditions change dramatically in preparing for the monsoon onset. Here we notice a significant increase of atmospheric relative humidity and its dominant contribution to abrupt increase of cyclone frequency. In fact, the rapid accumulation of water vapor over the BoB and its neighborhood is also the precondition of monsoon onset over the BoB and favors the BoB as the region where Asian Boreal Summer Monsoon is earliest established (Li et al. 2011). Therefore the high season of cyclone during April-May is closely associated with the boreal summer monsoon onset over the BoB, which will be further discussed in the next section.

The first decrease of cyclone frequency occurs in June-July compared with the level in April-May (Figs. 2 and 3). The net effect (GPI change: -0.29) is that the combined effect of atmospheric vertical wind shear (contribution to GPI change: -0.66), vorticity (contribution to GPI change: -0.24) and potential intensity (contribution to GPI change: -0.14) overwhelms the water vapor effect (contribution to GPI change: +0.75). We emphasize the important role relative humidity plays during this period. The presence of rich water vapor can be easily understood since the evaporation process is very active under the strong southwest monsoon. The low cyclone frequency during boreal summer occurs due to the complex interplay among the four different processes, not due to the strong vertical wind shear alone. Gray (1968) has pointed that the cyclone frequency minimum in the BoB during the boreal summer monsoon is due to the very strong vertical wind shear. Here we provide a more quantitative picture, that is, the vertical wind shear does play an important role but it alone is not enough. It has to work together with absolute vorticity and potential intensity parameters to overcome the relative humidity effect.

The second increase of cyclone frequency occurs in October-November with reference to the level in August-September. It is mainly attributed to the decrease of the vertical shear. This environmental factor alone contributes to 91% of the GPI increase. In comparison to the first increase of cyclone frequency in April-May, we emphasize that their underlying physical processes are totally different. The dramatic increase of atmospheric relative humidity controls the first period and the immediate decrease of vertical wind shear dominates the second period.

The second decrease of cyclone frequency occurs in December-January with reference to the level in October-November. This is primarily caused by the decrease of the environmental relative humidity (contribution in percentage of 75%) and relative vorticity (contribution in percentage of 22%). The period of December-January is dominated by the boreal winter northeast monsoon, which is much weaker and drier than the boreal southwest monsoon.

4. Contrast with other ocean basins

To better understand the contrast of cyclone annual cycle in the BoB and other oceanic basins, we further extend a similar analysis to other basins. For simplicity, we only show the results in the northern hemisphere regions, including the AS, the WNP, the ENP and the NATL.

As shown in Fig. 2g, the AS shows a similar bimodal feature as in the BoB. This is consistent with earlier analysis of the whole North Indian Ocean (Camargo et al. 2007). However, the mismatch between the GPI and cyclone occurrence in the AS is much larger than those in other basins. As discussed in Camargo et al. (2007), this kind of mismatch is especially significant in a small basin due to less cyclone numbers. To guarantee the statistical significance of the analyzed results, the AS and BoB are normally combined together as one North Indian basin in such analysis (Camargo et al. 2007). A diagnosis of the individual contributions for the AS was done and given in Tab. 2d. As a first order of approximation, the dominant processes for the suppressed cyclone activity in the AS during the boreal summer monsoon are shown to be the same with those in the BoB. It seems the dominant processes for the two peaks in the AS are different from those in the BoB. However, due to the large mismatch of GPI and cyclone occurrence, the diagnosis of the two peak period listed in Tab. 2d may be not robust.

The WNP, ENP and NATL basins all have a single peak in the annual cycle of the cyclone frequency. A similar calculation is repeated for these regions, except on a 4-month basis. The 4-month basis is chosen simply due to the fact that this is sufficient to resolve the evolution of the single peak. The quantitative contributions from the four factors in determining the increasing phase (from Feb-Mar-Apr-May to Jun-Jul-Aug-Sep) and the decreasing phase (from Jun-Jul-Aug-Sep to Oct-Nov-Dec-Jan) are calculated. The diagnosis results are listed in Table 2. The three basins with similar cyclone behavior also share the similar controlling physical processes. For both the increase and decrease phases, the environmental vertical wind shear and the relative humidity are always two leading factors, which are comparable in intensity, work in the same direction and collectively contribute over 80% of the total. In general, the governing processes for the cyclone activities in the WNP, ENP and NATL are simpler than those in the BoB where the monsoon climate dominates.

5. Observed cap of the vertical wind shear

The GPI diagnosis above reveals the geographically dependent features of vertical wind shear. During the boreal summer, the environmental vertical shear tends to reduce the cyclone genesis in the BoB, while it tends to increase the TC genesis frequency over the WNP, ENP and NATL. A natural question is what the observed upper shear limit for cyclogenesis is in different ocean basins. This motivates us to examine the caps of background vertical wind shear in the four basins.

Fig. 4 shows the climatologic mean annual cycle of the vertical shear, together with the scattering diagrams of all the cyclones expressed by their categories and the corresponding background vertical wind shear when they reached their maximum intensity, over the BoB, WNP, ENP and NATL. Firstly, the seasonal cycle of vertical wind shear over monsoon oceans (including the BoB and WNP) shows a semi-annual feature while an annual feature dominates over trade wind oceans (including the ENP and NATL). The semi-annual character over the BoB shows large winter-summer asymmetry, with maximum vertical shear (around 30 m s^{-1}) in summer and very weak shear (around 10 m s^{-1}) in winter. Although also dominated by a monsoon climate, the WNP has a different semi-annual feature from the BoB; it shows a winter-summer symmetry with a relative weak peak intensity at about 25 m s^{-1}. The ENP and NATL show a single peak in boreal winter and a single minimum in boreal summer. It is known that the large environmental vertical shear tends to disrupt development of TC warm core. The semi-annual and annual features help to explain the double peaks in the BoB and a single peak in the ENP and NATL, but they cannot explain why the WNP also shows a single peak in its annual cycle of cyclone frequency. This may be related to the different caps of vertical wind shear for cyclone formation in different regions.

The basin dependent caps of vertical wind shear for cyclone formation are shown in the right panel of Fig. 4, based on historical data during the period of 1981-2009. Here each blue star in Fig. 4 represents the 20-day low-pass filtered large-scale vertical shear value at the time when a cyclone reached its maximum intensity. The blue horizontal line represents the vertical shear threshold, above which there is no historical TC genesis. The red line represents the vertical shear cap for super typhoons (category 4 or above).

The analysis above indicates that the vertical shear caps for cyclone formation are different in different tropical basins. The cap is greatest in the WNP (37 m s^{-1}), followed by the NATL (32 m s^{-1}), BoB (24 m s^{-1}) and ENP (22 m s^{-1}). This is however not surprising since the background moisture, SST and circulation fields differ markedly in different basins. For example, the WNP is the region hosting the highest SST and the monsoon trough. Under such a favorable environment, TCs may form under a relatively large vertical shear. We will not further discuss the underlying mechanisms of the region-dependent caps of vertical wind shear, which is beyond the scope of the present paper. However, we will use the observed thresholds to understand the different cyclone behaviors in various regions.

Applying the observed vertical wind shear caps in cyclones to each basin, one can see clearly that in boreal summer the background vertical shears are far below the cap values over the WNP, ENP and NATL. This means that TC genesis in these basins is not restricted at all by this parameter. The situation, however, is very different in the BoB. In most of the summer season, the background vertical shear exceeds this cap.

This helps explain why BoB TCs occur quite infrequently in boreal summer.

6. Comparison between two peak seasons

As an extension of the bimodal analysis of the BoB cyclones, we can further compare the two peaks shown in Fig. 2. It appears that the majority of the historical super cyclones (category 4 or above) occurred within the first peak season (especially in April), although there were more cyclones during the second peak season. We now analyse the underlying processes.

It is found that much higher water vapor during October-November is the major cause of higher cyclone frequency in the second peak. Fig. 5 shows that relative humidity in October-November is much higher than that in April-May. The strength of vertical wind shear during April-May and October-November, on the other hand, is almost the same. The difference of relative humidity between the two peak periods is primarily attributed to the circulation asymmetry between northern fall and spring. In northern fall (spring) the climatologic low-level flow in northern Indian Ocean resembles the summer (winter) circulation with dominant southwesterly (northeasterly) winds. This leads to a difference in moisture advection in the region. As a result, higher humidity occurs right after the monsoon season, compared to that prior to the monsoon. This relative humidity effect may be further inferred from Table 1, which shows a small decrease of relative humidity (about -5%) from Aug-Sep to Oct-Nov. Thus it can be deduced that higher relative humidity in October-November favors more cyclone genesis in comparison with the case in April-May.

Favorable genesis conditions do not guarantee the subsequent strong development of a cyclone. Our diagnosis suggests that two factors may contribute to the predominance of super cyclones in April-May. Firstly, there is a marked difference in the upper 300m ocean heat content between the two peak periods. The ocean heat content is larger in boreal spring than in boreal fall, particularly in the northwestern part of the BoB (Fig. 6a). While TC genesis does not necessarily rely on what happens below the ocean mixed layer, the life evolution of a TC and in particular its rapid intensification do depend on the ocean heat content condition, in particular when a cyclone moves slowly (Wada and Chan 2008; Lin et al. 2009).

A concept of the PI was introduced by Emanuel (1988), and represents an upper bound or a thermodynamic limit for TC intensity. Wing et al. (2007) examined the interannual relationship between the potential and actual TC intensity and found that they are in general consistent. Here, to consider the ocean heat content effect, a modified potential intensity index is introduced as following:

$$V_{pot} = \sqrt{C_p (T_{HC} - T_o) \frac{T_{HC}}{T_o} \frac{C_k}{C_D} (\ln\theta^*_{HC} - \ln\theta_e)} \qquad (6),$$

where T_{HC} =γ×HC represents an equivalent upper-ocean temperature, HC denotes a vertically integrated (0-300m) heat content, and γ is a constant coefficient and in the present study it is assigned to a value of 0.005 m^{-1}. θ^*_{HC} denotes saturation equivalent potential temperature, in which T_{HC} is used to replace SST for calculation. The other parameters are same as in equation (1).

Fig. 6b shows the modified PI index at each month. For comparison we also show the time series of the original SST-based PI index. It turns out that both the indices show a greater PI value in April-May than in October-November. This suggests that more intensive cyclones are likely to occur in April-May than in October-November.

The second factor is attributed to the difference in the ISO activity. April-May is the time of monsoon onset over the BoB, which is normally triggered by the first-branch northward-propagating ISO (Li et al. 2012). The low-level cyclonic circulation, boundary convergence and rich moisture associated with the northward-propagating ISO, all dramatically favor the rapid development of the cyclones over the BoB and sometimes make them into super cyclones. A careful examination of the timing of BoB super cyclones during 1981-2009 indicates that five out of the total seven took place when they were in phase with the first-branch northward-propagating ISOs over the BoB (Fig. 7a). The other two cases were in phase with the second branch of northward propagating ISOs. The ISO low-level flow and associated moisture condition may accelerate TC development through barotropic energy conversion (Hsu et al. 2011a,b) or the modulation of diabatic heating and the surface latent heat fluxes (Zhou and Li 2010; Hsu and Li 2011). The ISO can strengthen TC intensity through the deepening of the background moist layer (i.e., increase of moisture content from lower troposphere to middle troposphere) and the increase of the background low-level cyclonic vorticity (Camargo et al. 2009; Kikuchi and Wang 2010; Yanase et al. 2010, 2012). By comparing the 20-60-day variance in both the transitional seasons, we found that the ISO variance is indeed greater in April-May than in October-November (Fig. 7b). Therefore, both the greater ISO variability and a higher modified PI index in Apr-May are consistent with the fact that the peak season of super cyclones occurred in the first peak period.

7. Conclusion and discussion

In this study we investigated the cause of the double peaks of TC activity in the BoB. A genesis potential index (GPI) was used to examine the influence of large scale environmental factors on the cyclone genesis, including the absolute vorticity, the vertical shear, the relative humidity and the potential intensity. The GPI diagnosis shows that this index well captures the observed TC annual cycle characteristics in all major basins.

A total differential method is used to separate the relative contribution of each factor in shaping the bimodal feature of cyclone frequency. It is found that the relative humidity increase in April-May is the dominant factor for the first cyclone season and the decrease of the vertical wind shear in October-November accounts for the second cyclone season. The cyclone minimum during the boreal summer monsoon is due to the complex interplay among all four factors. The forcing of vertical wind shear, vorticity and potential intensity works collectively and hence overwhelms the cyclone-favorable high relative humidity. The vertical wind shear plays an important role in causing the cyclone minimum in boreal summer, as Gray (1968) mentioned, but is not a sole factor. The cyclone minimum during the boreal winter is mainly controlled by the presence of dry air.

The comparison between the BoB and other basins, including the WNP, ENP and

NATL, reveals that the basins with a single peak in th cyclone annual cycle share the similar underlying environmental conditions. The relative humidity and vertical wind shear are always two leading factors with comparable intensity and same sign. The environmental conditions for the BoB are totally different. There is only one dominant factor in pre-monsoon (relative humidity), post-monsoon (vertical wind shear) and winter monsoon (relative humidity) periods. BoB boreal summer is most complex when all the four factors come into play.

It is found that the cap of vertical wind shear for TC formation is basin-dependent. Due to strong South Asian summer monsoon, the vertical wind shear exceeds the observed cap in the BoB and hence restricts the development of the cyclone. This limiting condition does not exist in the WNP, ENP and NATL.

Finally we analyzed the cause of cyclone frequency difference in two transitional seasons over the BoB. The higher background relative humidity during October-November than in April-May is the major factor that contributes to more frequent cyclone genesis in October-November. In contrast to the TC frequency, the most intense cyclones are observed to occur in April-May rather than in October-November. It is argued that the following two factors may contribute to such a difference. Firstly, the greater ocean heat content may lead to a greater TC potential intensity. Secondly, the occurrence of the first-branch northward-propagating ISO along with stronger ISO variability in April-May may favor the rapid intensification of weak TCs into intense cyclones through its impact on background relative humidity and vorticity.

The major difference between previous studies such as Yanase et al. (2012) and the current work is that the former did not quantitatively show the relative contribution of each of the GPI terms. For example, Yanase et al. (2012) and other previous studies emphasized the effect of vertical shear in causing the GPI minimum in boreal summer. This differs from our result. By evaluating the contribution from each of the four GPI terms, we note that the enhanced vertical shear effect (-0.66) from spring to summer alone cannot offset the increased RH effect (+0.75) (Table 1). Only when two other environmental factors, the vorticity effect (-0.24) and the SST effect (-0.14), are included, would the GPI become negative (relative to the annual mean value). Therefore, the summer GPI minimum results from combined vertical shear, vorticity and SST effects. Another difference is that the current study addresses the cause of the GPI difference between two transitional seasons.

A unique aspect of the current diagnosis approach is to provide a quantitative assessment of the contribution from each of the environmental parameters using equation (5). It is worth mentioning that an approximation was made in deriving the equation, that is, we assumed constant coefficients for α_1, α_2, α_3 and α_4. This assumption is equivalent to a small ratio of delta (Term X) to bar (Term X), where X is 1 to 4. To validate whether or not such an approximation is reasonable, we calculated the ratio of delta (Term X) to bar (Term X) for each month, and found that the ratio is indeed small (about 0.1) for most of months except for only a couple of months in which the ratio can be as large as 0.3. This indicates that the approximation used in the linear derivation is acceptable to the lowest order.

The purpose of section 5 is to reveal the observed upper limit of the background vertical shear for TCs. Due to different mean state conditions (such as SST, moisture and other environmental parameters), the upper limit value of the vertical shear could be different in different basins. This is why we identify the observed upper bound for intense cyclones and all TCs at each basin. This observational analysis provides additional useful information about TC behavior at individual basins.

A question related to the newly formulated PI index is whether or not one should include the vertical shear effect. We noted that averaged vertical shear (10.3 m/s) in the BoB in April-May is slightly greater than that (9.9 m/s) in October-November. If one includes the vertical shear effect (using the same formula as in Equation 1) in the PI formula, one can still derive the same conclusion that the PI in April-May is greater than that in October-November. However, the PI difference between the two transitional seasons becomes smaller. This indicates that the vertical shear plays a negative role in contributing to the observed difference in intense cyclone formation between April-May and October-November. Because the original meaning of the PI defined by Emanuel (1988) and Holland (1997) represented the thermodynamic upper limit of TC maximum potential intensity, which did not include dynamical effects, we excluded the vertical shear effect in the current PI formula. Nevertheless, inclusion of both dynamic and thermodynamic effects is needed for a complete understanding of the seasonal evolution of TC formation.

Acknowledgements. This work was supported by Chinese MoST grant No.

2010CB950303 and NSF grant No.40730842. TL acknowledged a support by ONR grant N000140810256.

Reference:

Camargo, S. J., K. A. Emanuel, and A. H. Sobel, 2007: Use of a genesis potential index to diagnose ENSO effects on tropical cyclone genesis. *J. Clim.*, **20**, 4819–4834.

Camargo, S. J., M.C. Wheeler, and A. H. Sobel, 2009: Diagnosis of the MJO modulation of Tropical Cyclogenesis Using an Empirical Index. *J. Atmos. Sci.*, **66** , 3061–3074.

Emanuel, K. A., 1986: An air-sea interaction theory for tropical cyclones I: Steady-state maintenance, *J. Atmos. Sci.*, **43**, 585–604.

Emanuel, K. A., 1987: The dependence of hurricane intensity on climate. *Nature*, **326**, 483– 485.

Emanuel, K. A., 1988: The maximum intensity of hurricanes. *J. Atmos. Sci.*, **45**, 1143–1155.

Emanuel, K. A., 1995: Sensitivity of tropical cyclones to surface exchange coefficients and a revised steady-state model incorporating eye dynamics. *J. Atmos. Sci.*, **52**, 3969– 3976.

Emanuel, K. A., 2000: A statistical analysis of tropical cyclone intensity. *Mon. Wea. Rev.*, **128**, 1139–1152.

Emanuel, K. A., and D. S. Nolan, 2004: Tropical cyclone activity and global climate. Preprints, 26th Conf. on Hurricanes and Tropical Meteorology, Miami, FL, *Amer. Meteor. Soc.*, 240–241.

Emanuel, K. A., 2005: Increasing destructiveness of tropical cyclones over the past 30 years. *Nature*, **436**, 686–688, doi:10.1038/nature03906.

Evan, A. T., and S. J. Camargo, 2011: A Climatology of Arabian Sea Cyclonic Storms. *J. Clim.*, **24**, 140–158, doi: 10.1175/2010JCLI3611.1.

Gray, W. M., 1968: Global view of the origin of tropical disturbances and storms. *Mon. Wea. Rev.*, **96**, 669–700.

Gray, W. M., 1979: Hurricanes: Their formation, structure and likely role in the general circulation, in *Meteorology over the Tropical Ocean*s. edited by D. B. Shaw, *R. Meteorol. Soc.*, Bracknell, U. K., 155–218.

Henderson, S. A., and Coauthors, 1998: Tropical cyclones and global climate change: A Post-IPCC Assessment. *Bulletin of American Meteorological Society*, **70**, 19-38.

Holland, G. J., 1997: The Maximum Potential Intensity of Tropical Cyclones. J. Atmos. Sci., 54, 2519–2541.

Hsu, P. C., T. Li, and C H. Tsou, 2011a: Interactions between boreal summer intraseasonal oscillations and synoptic-scale disturbances over the western North Pacific. Part I: Energetics diagnosis. *J. Clim*, **24**, 927-941.

Hsu, P. C., and T. Li, 2011b: Interactions between boreal summer intraseasonal oscillations and synoptic-scale disturbances over the western North Pacific. Part II: Apparent heat and moisture sources and eddy momentum transport. *J. Clim.*, **24,** 942–961.

Kikuch,K., B. Wang and H. Fudeyasu, 2009: Genesis of tropical cyclone Nargis Revealed by multiple satellite observations, *Geophys. Res. Lett*. **36**, L06811, doi:10.1029/2009GL037269.

Kikuch, K. and B. Wang, 2010: Formation of tropical cyclones in the North Indian Ocean associate with two types of tropical intraseasonal oscillation modes, *J . Meteorological Society of Japan*, vol.**88**, No.**3**, 475–496.

Landsea, C. W., B. A. Harper, K. Hoarau, and J. A. Knaff, 2006: Can we detect trends in extreme tropical cyclones?. *Science*, **313**, 452–454, doi:10.1126/science.1128448.

Li, K., W. Yu, and T. Li, 2011: Structures and Mechanisms of the First-Branch Northward-Propagating Intraseasonal Oscillation over the Tropical Indian Ocean. Manuscript submitted to *Climate Dynamics,* in press.

Li, T., M. Kwon, M. Zhao, J. Kug, J. Luo, and W. Yu, 2010: Global warming shifts Pacific tropical cyclone location, *Geophys. Res. Lett*., **37**, L21804, doi:10.1029/2010GL045124.

Li, T., 2012: Synoptic and climatic aspects of tropical cyclogenesis in western North Pacific in Cyclones: Formation, triggers and control, edited by K. Oouchi and H. Fudevasu, Noval Science Publishers, in press.

Lin, I. I., C. H. Chen, I. F. Pun et al., 2009: Warm ocean anomaly, air sea fluxes, and the rapid intensification of tropical cyclone Nargis (2008), *Geophys. Res. Lett*., **36**, L03817, doi:10.1029/2008GL035815.

Lin, I. I., I. F. Pun and C. C. Wu, 2009: Upper-ocean thermal structure and the western North Pacific category 5 typhoon. Part II: Dependence on transitional speed. *Mon. Wea. Rev*., **137**, 3744–3757.

Lyon, B., H. Cristi, E.R. Verceles, F.D. Hilario, and R. Abastillas, 2006: Seasonal reversal of the ENSO rainfall signal in the Philippines. *Geophys. Res. Lett.*,**33**, L24710, doi:10.1029/2006GL028182.

Lyon, B. and S.J. Camargo, 2008: The seasonally-varying influence of ENSO on rainfall and tropical cyclone activity in the Philippines, *Clim. Dyn.*, **32**, doi:10.1007/s00382-008-0380-z.

McPhaden, M. J., G. R. Foltz, T. Lee, et al., 2009: Ocean-atmosphere interactions during cyclone Nargis, *Eos Trans. AGU*, **90(7)**, 54–55.

Singh, O. P., T. M. Ali Khan and M. S. Rahman, 2000: Changes in the frequency of tropical cyclones over the North Indian Ocean. *Meteorol. Atmos. Phys.*, **75**, 11–20.

Singh, O. P., T. M. Ali Khan and M. S. Rahman, 2001: Has the frequency of intense tropical cyclones increased in the north Indian Ocean? *Research Communications*, **80**, 575–580.

Wada, A. and J. C. L. Chan, 2009: Relationship between typhoon activity and upper ocean heat content, *Geophys. Res. Lett.*, **35**, L17603, doi:10.1029/2008GL035129.

Webster, P. J., G. J. Holland, J. A. Curry, and H. R. Chang, 2005: Changes in tropical cyclone number, duration, and intensity in a warming environment. *Science*, **309**, 1844–1846, doi:10.1126/science.1116448.

Webster, P. J., 2008: Myanmar's deadly daffodil. *Nature Geoscience*, **1**, doi: 10.1038/nego257.

Wing, A. A., A. H. Sobel and S. J. Camargo, 2007: Relationship between the potential and actual intensities of tropical cyclones on interannual time scale. *Geophys. Res. Lett.*, **34**, L08810, doi:10.1029/2006GL028581.

Yanase, W., H. Taniguchi and M. Satoh, 2010: The Genesis of Tropical Cyclone Nargis (2008): Environmental modulation and numerical predictability. *J . Meteorological Society of Japan*, **88**, 497–519.

Yanase, W., M. Satoh, H. Taniguchi and H. Fujinami, 2012: Seasonal and intra-seasonal modulation of tropical cyclogenesis environment over the Bay of Bengal during the extended summer, *J. Clim.*, **25**, 2914–2930.

Zhou, C. and T. Li, 2010: Upscale feedback of tropical synoptic variability to intraseasonal oscillations through the nonlinear rectification of the surface latent heat flux. *J. Climate*, **23**, 5738–5754.

Table Captions

Table 1:

Table 1: Contributions to δGPI in the BoB during increasing and decreasing formation periods.

Table 2: Contributions of each term to δGPI in the (a) WNP, (b) ENP, (c) NATL and (d)AS

Table 3: the GPI difference between April-May and October-November

Figure Captions

Fig. 1 Global distribution of cyclone genesis locations during 1981-2009, the Genesis Potential Index (GPI) is calculated in the region within blue rectangle for capturing the character of the annual cycle in each ocean basin. The green, yellow, red, blue, magenta, cyan and gray indicate the category of TCs: -1, 0, 1, 2, 3, 4 and 5, respectively. According to Saffir-Simpson scale, grades -1 and 0 denote tropical depression and tropical storm, and grade 1 to 5 represents different typhoon strength, ranging from category 1 to category 5.

Fig. 2 Monthly TC numbers (column) during 1981-2009 in the (a) BoB, (b) WNP, (c) ENP, (d) NATL, (e) SIO and (f) WSP, respectively. The dark blue, blue, light blue, green, yellow, red and dark red indicate the category of TCs: -1, 0, 1, 2, 3, 4 and 5, according to Saffir-Simpson scale. The overlaid gray curves represent the climatological monthly GPI values. The left vertical-axis is for TC number and the right vertical-axis is for the GPI value.

Fig. 3 Climatologic monthly contributions of each term at right-hand side of equation (5) (denoted by a specified color bar) and their sum in the BoB. The solid line is the sum of the right-hand side terms using coefficients $\alpha_1 = \overline{\mathrm{Term2}} \cdot \overline{\mathrm{Term3}} \cdot \overline{\mathrm{Term4}}$, $\alpha_2 = \overline{\mathrm{Term1}} \cdot \overline{\mathrm{Term3}} \cdot \overline{\mathrm{Term4}}$, $\alpha_3 = \overline{\mathrm{Term1}} \cdot \overline{\mathrm{Term2}} \cdot \overline{\mathrm{Term4}}$, and $\alpha_4 = \overline{\mathrm{Term1}} \cdot \overline{\mathrm{Term2}} \cdot \overline{\mathrm{Term3}}$. The gray dashed line is the sum of the right-hand side terms using coefficients $\alpha_1 = \overline{\mathrm{Term2} \cdot \mathrm{Term3} \cdot \mathrm{Term4}}$, $\alpha_2 = \overline{\mathrm{Term1} \cdot \mathrm{Term3} \cdot \mathrm{Term4}}$, $\alpha_3 = \overline{\mathrm{Term1} \cdot \mathrm{Term2} \cdot \mathrm{Term4}}$, and $\alpha_4 = \overline{\mathrm{Term1} \cdot \mathrm{Term2} \cdot \mathrm{Term3}}$. The red dashed line is the observed $\delta\mathrm{GPI}$ value.

Fig. 4 Climatologic annual cycle of the vertical shear (unit: m s^{-1}) of background wind (green dots) and the standard deviation (black bar) during 1981-2009 over the BoB, WNP, ENP and NATL (left panels), and scatter diagrams of the background (20-day low-pass filtered) vertical shear at the time when a TC reached its maximum (right panels). The blue line denotes a vertical shear cap in each basin, and the red line denotes a vertical shear cap for super typhoons in each basin.

Fig. 5 Difference (October-November minus April-May) of the environmental relative humidity at 600hPa (top, a) and the climatologic annual cycle (green dots) and standard deviation (blue bar) of the relative humidity in the BoB (bottom, b).

Fig. 6 (Top, a) Difference (Apr-May minus Oct-Nov) of the upper-ocean heat content (unit: °C m). (Bottom, b) The PI indices (unit: m s^{-1}) calculated based on an equivalent upper-ocean temperature (red) and SST (blue).

Fig. 7 (Top, a) Composite map of the monsoon onset over the BoB, associated with the first-branch northward-propagating ISO; Purple dots denote the time (relative to the monsoon onset time) and latitude of intense TC (Category 4 or 5) when it reached its maximum intensity. Green dots denote the genesis time and latitude of these super cyclones. Shading and contour show the OLR averaged between 85E and 95E. The vector represents the surface wind averaged between 85E-95E. The Y-axis is latitude and x-axis denotes a relative time, with day 0 denoting the time when monsoon onset occurs over the BoB. (Bottom, b) Difference (Apr-May minus Oct-Nov) of standard deviation of 20-60-day band-pass filtered OLR fields, calculated based on the 29-yr (1981-2009) data.

Table 1: Contributions toδGPI in the BoB during increasing and decreasing formation periods

	δGPI	δterm 1	δterm 2	δterm 3	δterm 4
FM→AM	+0.52	+0.02 (+4%)	0 (0%)	+0.45 (+87%)*	+0.05 (+9%)
AM→JJ	-0.29	-0.24 (+85%)	-0.66 (+229%)*	+0.75 (-260%)	-0.14 (+46%)
AS→ON	+0.98	+0.14 (+14%)	+0.89 (+91%)*	-0.05 (-5%)	0 (0%)
ON→DJ	-1.39	-0.31 (+22%)	-0.03 (+2%)	-1.03 (+75%)*	-0.02 (+1%)

Table 2: Contributions of each term toδGPI in the (a) WNP, (b) ENP, (c) NATL and (d)AS

(a)	δGPI	δterm 1	δterm 2	δterm 3	δterm 4
MAMJ→JASO	+1.66	+0.16 (+10%)	+0.66 (+40%)*	+0.63 (+37%)	+0.21 (+13%)
JASO→NDJF	-1.99	-0.20 (+10%)	-0.67 (+34%)	-0.88 (+44%)*	-0.24 (+12%)

(b)	δGPI	δterm 1	δterm 2	δterm 3	δterm 4
FMAM→JJAS	+2.75	+0.14 (+5 %)	+1.14 (+42%)	+1.43 (+52%)*	+0.04 (+1%)
JJAS→ONDJ	-2.46	-0.19 (+8%)	-0.89 (+36%)	-1.21 (+49%)*	-0.17 (+7%)

(c)	δGPI	δterm 1	δterm 2	δterm 3	δterm 4
MAMJ→JASO	+0.66	+0.06 (+9%)	+0.25 (+38%)	+0.27 (+40%)*	+0.08 (+13%)
JASO→NDJF	-0.56	-0.06 (+11%)	-0.25 (+44%)	-0.27 (+48%)*	+0.02 (-3%)

(d)	δGPI	δterm 1	δterm 2	δterm 3	δterm 4
MA→MJ	+0.06	+0.03(+57%)	-0.33(-588%)	+0.38(+669%)	-0.02(-38%)

MJ→JA	-0.16	-0.27(+171%)	-0.55(+349%)	0.82(-520%)	-0.16(+100%)
AS→ON	+0.20	+0.50(+249%)	+0.47(+241%)	-0.87(-432%)	+0.08(+42%)
ON→DJ	-0.35	-0.12(+35%)	-0.11(+30%)	-0.12(+35%)	0

Table 3: The GPI difference between April-May and October-November

	δGPI	δterm 1	δterm 2	δterm 3	δterm 4
AM→ON	+0.72	+0.07 (+10%)	+0.03 (+5%)	+0.82 (+113%)*	-0.20 (-28%)

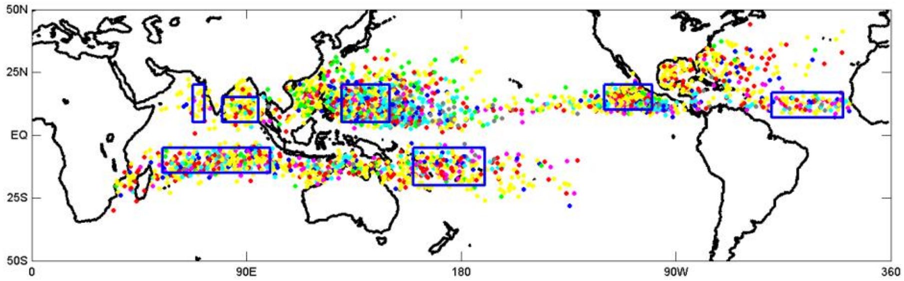

Fig. 1 Global distribution of cyclone genesis locations during 1981-2009, the Genesis Potential Index (GPI) is calculated in the region within blue rectangle for capturing the character of the annual cycle in each ocean basin. The green, yellow, red, blue, magenta, cyan and gray indicate the category of TCs: -1, 0, 1, 2, 3, 4 and 5, respectively. According to Saffir-Simpson scale, grades -1 and 0 denote tropical depression and tropical storm, and grade 1 to 5 represents different typhoon strength, ranging from category 1 to category 5.

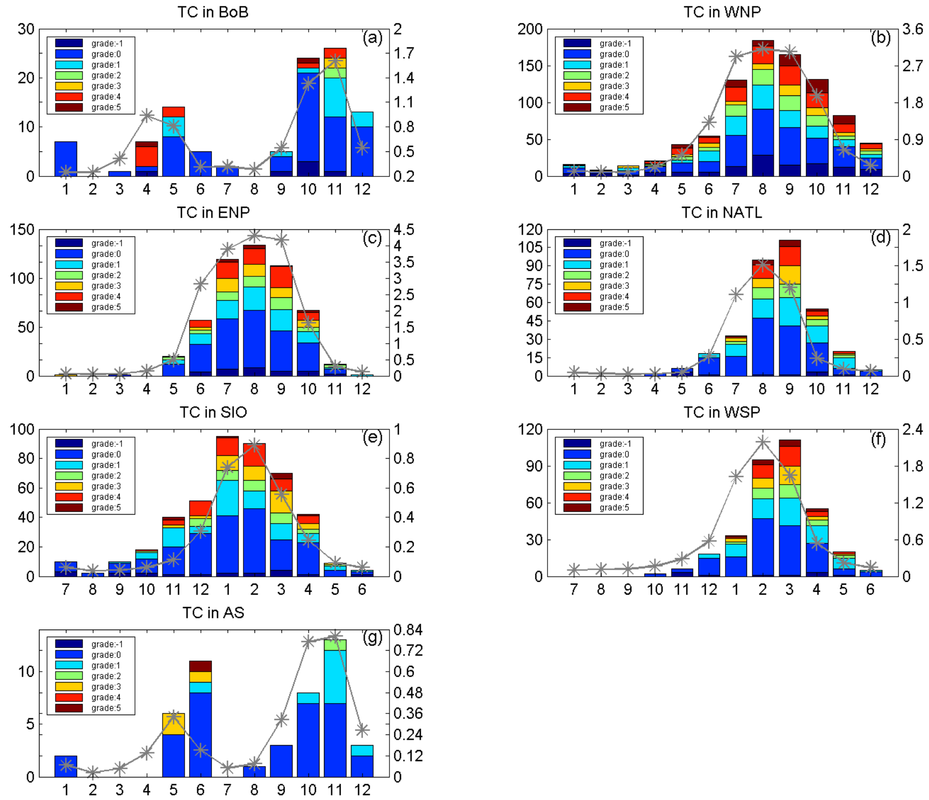

Fig. 2 Monthly TC numbers (column) during 1981-2009 in the (a) BoB, (b) WNP, (c) ENP, (d) NATL, (e) SIO and (f) WSP, respectively. The dark blue, blue, light blue, green, yellow, red and dark red indicate the category of TCs: -1, 0, 1, 2, 3, 4 and 5, according to Saffir-Simpson scale. The overlaid gray curves represent the climatological monthly GPI values. The left vertical-axis is for TC number and the right vertical-axis is for the GPI value.

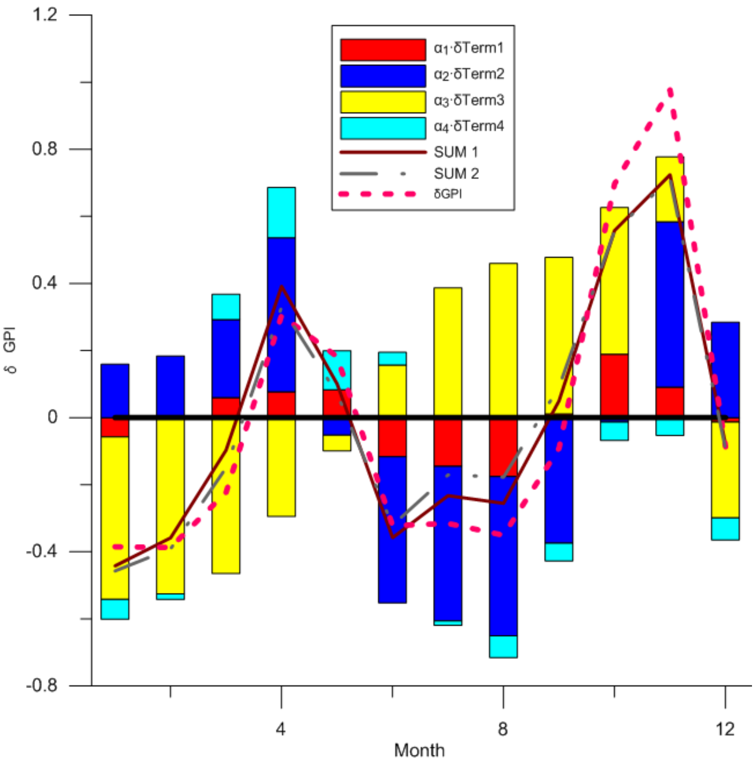

Fig. 3 Climatologic monthly contributions of each term at right-hand side of equation (5) (denoted by a specified color bar) and their sum in the BoB. The solid line is the sum of the right-hand side terms using coefficients $\alpha_1 = \overline{\mathrm{Term2}} \cdot \overline{\mathrm{Term3}} \cdot \overline{\mathrm{Term4}}$, $\alpha_2 = \overline{\mathrm{Term1}} \cdot \overline{\mathrm{Term3}} \cdot \overline{\mathrm{Term4}}$, $\alpha_3 = \overline{\mathrm{Term1}} \cdot \overline{\mathrm{Term2}} \cdot \overline{\mathrm{Term4}}$, and $\alpha_4 = \overline{\mathrm{Term1}} \cdot \overline{\mathrm{Term2}} \cdot \overline{\mathrm{Term3}}$. The gray dashed line is the sum of the right-hand side terms using coefficients $\alpha_1 = \overline{\mathrm{Term2} \cdot \mathrm{Term3} \cdot \mathrm{Term4}}$, $\alpha_2 = \overline{\mathrm{Term1} \cdot \mathrm{Term3} \cdot \mathrm{Term4}}$, $\alpha_3 = \overline{\mathrm{Term1} \cdot \mathrm{Term2} \cdot \mathrm{Term4}}$, and $\alpha_4 = \overline{\mathrm{Term1} \cdot \mathrm{Term2} \cdot \mathrm{Term3}}$. The red dashed line is the observed $\delta\mathrm{GPI}$ value.

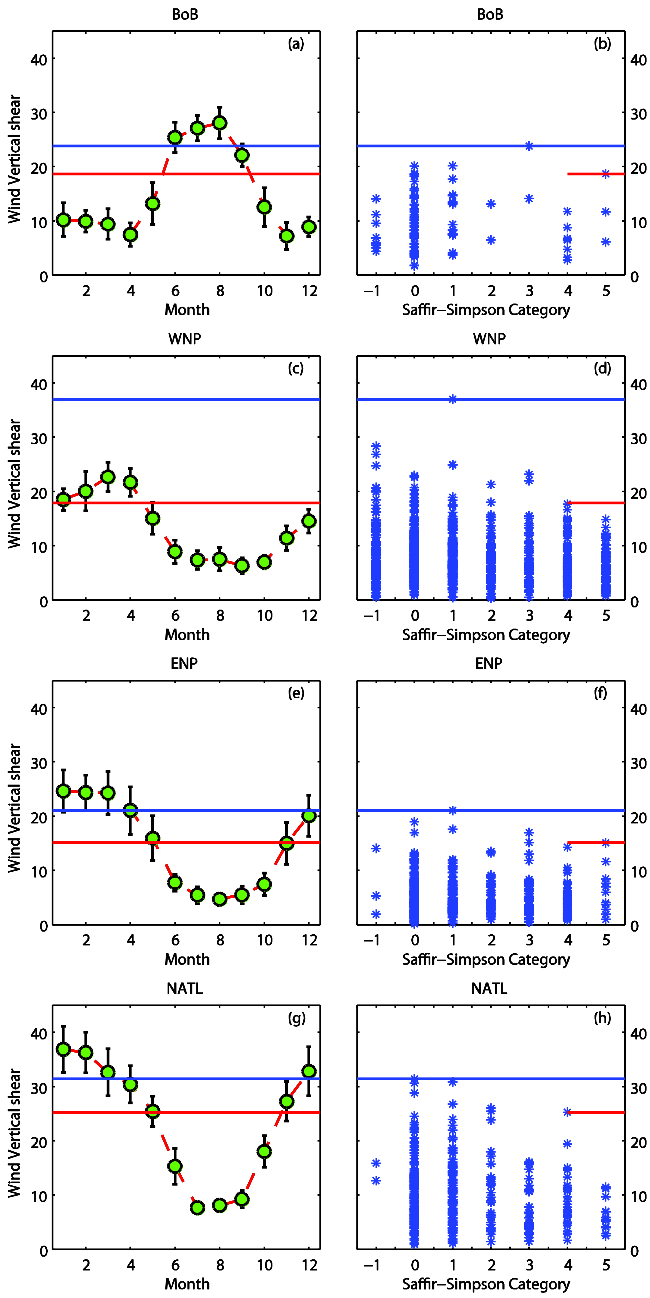

Fig. 4 Climatologic annual cycle of the vertical shear (unit: m s^{-1}) of background wind (green dots) and the standard deviation (black bar) during 1981-2009 over the BoB, WNP, ENP and NATL (left panels), and scatter diagrams of the background (20-day low-pass filtered) vertical shear at the time when a TC reached its maximum (right panels). The blue line denotes a vertical shear cap in each basin, and the red line denotes a vertical shear cap for super typhoons in each basin.

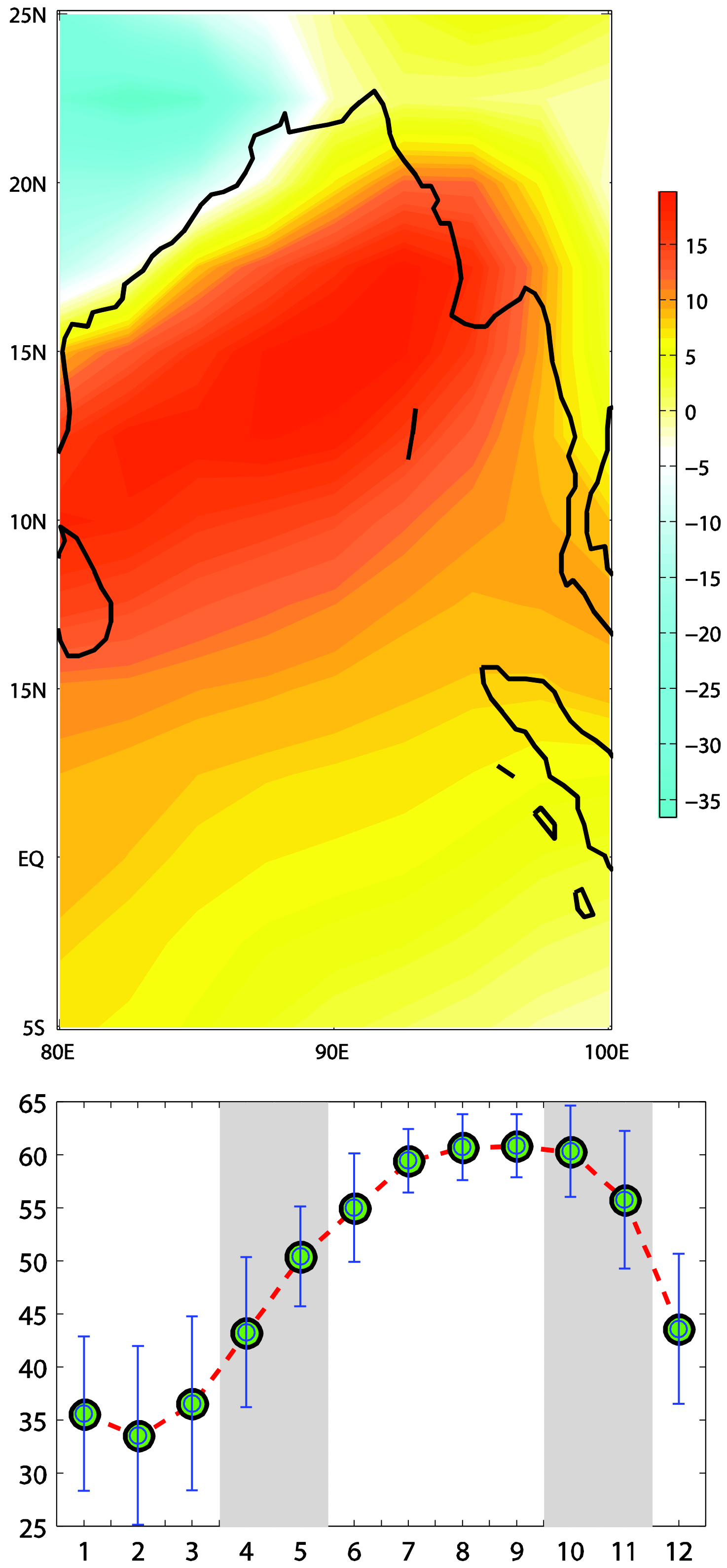

Fig. 5 Difference (October-November minus April-May) of the environmental relative humidity at 600hPa (top, a) and the climatologic annual cycle (green dots) and standard deviation (blue bar) of the relative humidity in the BoB (bottom, b).

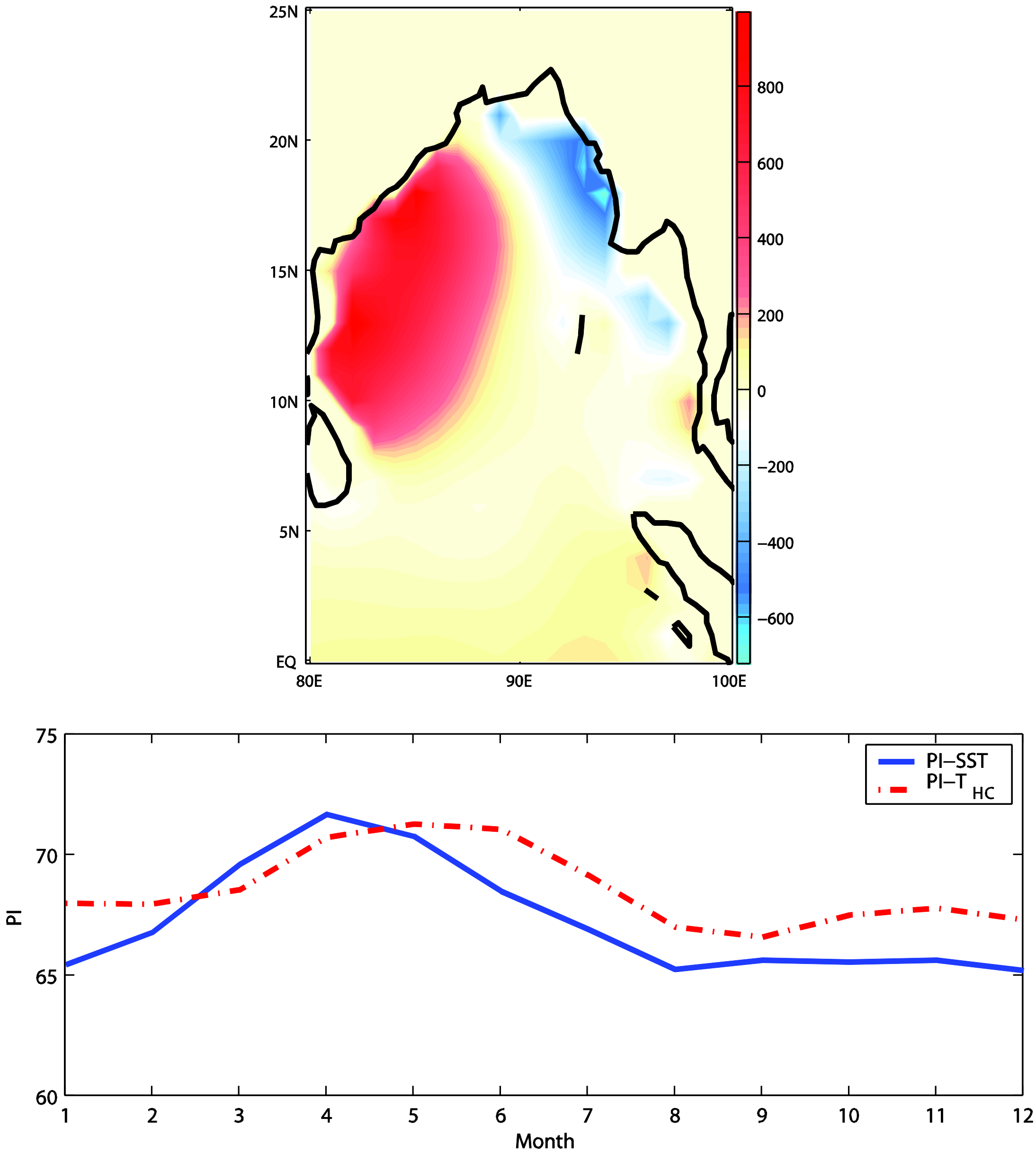

Fig. 6 (Top, a) Difference (Apr-May minus Oct-Nov) of the upper-ocean heat content (unit: °C m). (Bottom, b) The PI indices (unit: m s^{-1}) calculated based on an equivalent upper-ocean temperature (red) and SST (blue).

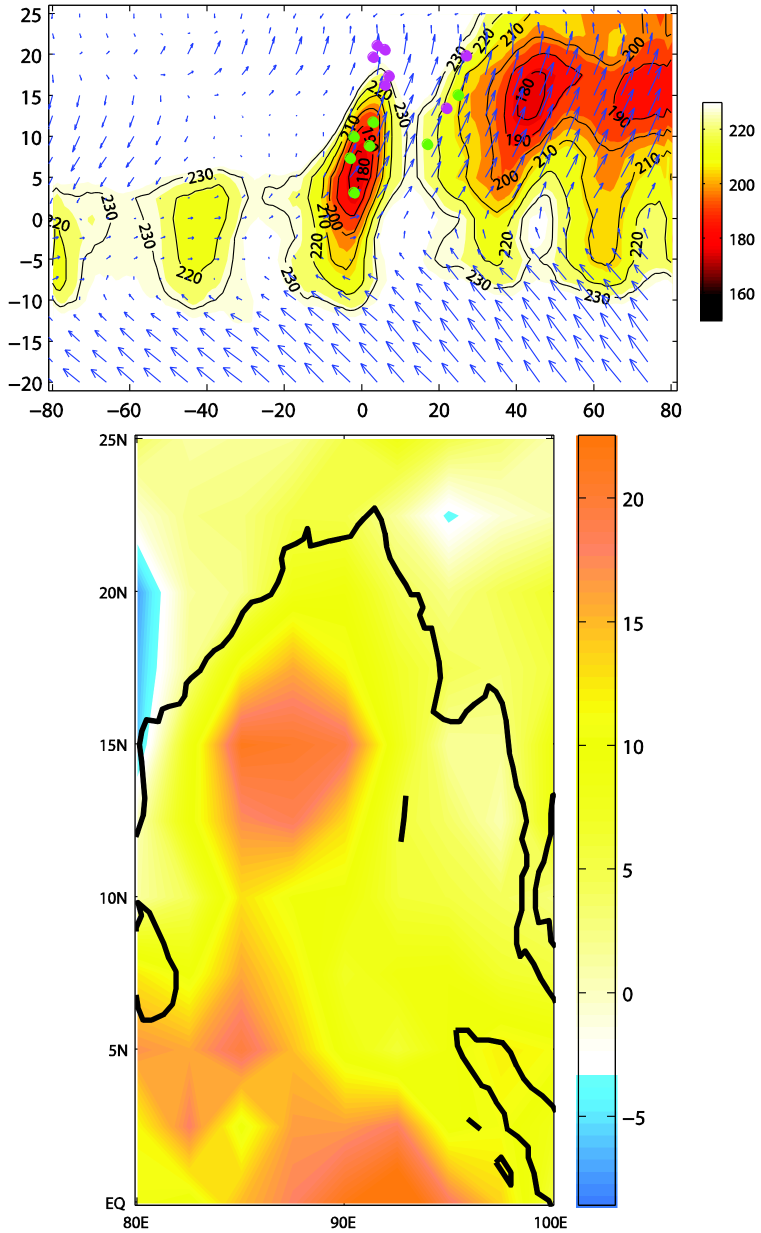

Fig. 7 (Top, a) Composite map of the monsoon onset over the BoB, associated with the first-branch northward-propagating ISO; Purple dots denote the time (relative to the monsoon onset time) and latitude of intense TC (Category 4 or 5) when it reached its maximum intensity. Green dots denote the genesis time and latitude of these super cyclones. Shading and contour show the OLR averaged between 85E and 95E. The vector represents the surface wind averaged between 85E-95E. The Y-axis is latitude and x-axis denotes a relative time, with day 0 denoting the time when monsoon onset occurs over the BoB. (Bottom, b) Difference (Apr-May minus Oct-Nov) of standard deviation of 20-60-day band-pass filtered OLR fields, calculated based on the 29-yr (1981-2009) data.